Catalysis Science & Technology

ROYAL SOCIETY OF CHEMISTRY

PAPER

View Article Online
View Journal | View Issue

Cite this: *Catal. Sci. Technol.*, 2024, **14**, 5439

Mechanism and structure–activity relationship of H_2 and CO_2 activation at the ZnO/Cu catalyst interface†

Xin Xin, [ab] Peng Gao [*abc] and Shenggang Li [*abcd]

$Cu/ZnO/Al_2O_3$ catalysts are the most well-known heterogeneous catalysts for the hydrogenation of CO and CO_2 into methanol. Herein, density functional theory calculations were performed to investigate the mechanism of H_2 activation and the effects of hydrogen spillover on CO_2 adsorption and activation at the interfacial site of the ZnO/Cu model catalyst, which was simulated by loading ZnO ribbons of different sizes on the Cu(111), Cu(100), and Cu(211) surfaces. The ZnO/Cu interface is found to facilitate the formation of H adsorbates from the dissociation of H_2 molecules, which promotes the facile formation of oxygen vacancy (V_O) sites in the ZnO component due to its reducibility and the hydrogen spillover effect. The resulting interfacial structure of the ZnO/Cu model catalyst can contain perfect, hydroxylated, and oxygen-vacancy-present ZnO sites, which may act as the adsorption and activation sites for CO_2. Further calculations show that molecular CO_2 adsorbed at the V_O site ($CO^*_{2\_V_O}$) can be efficiently activated by direct dissociation or hydrogenation to the HCOO* species. In addition, the smaller ZnO structure and less exposure of the Cu(211) facet facilitate hydrogen spillover and the formation of the interfacial V_O site. This study provides important insights into the structure–activity relationship for the active sites of the ZnO/Cu model catalyst and the mechanisms of CO_2 activation and hydrogenation.

Received 10th May 2024,
Accepted 27th July 2024

DOI: 10.1039/d4cy00604f

rsc.li/catalysis

1 Introduction

The use of fossil energy led to excessive emission of greenhouse gases especially carbon dioxide (CO_2), and the resulting global warming effect is threatening the sustainable development of mankind.[1–4] In recent years, CO_2 capture, utilization, and storage (CCUS) technologies have received increasing attention because of their potential for mitigating the severe consequences of excessive CO_2 emission and at the same time producing necessary fuels and valuable chemicals.[5–7] CO_2 hydrogenation is an effective approach for the synthesis of methanol,[8–11] which can be directly used as a fuel or fuel additive, or indirectly used as a chemical intermediate to further produce more advanced fuels and chemicals. $Cu/ZnO/Al_2O_3$ is the most widely studied catalyst for CO_2 hydrogenation to methanol due to its low cost and high activity, and the industrial $Cu/ZnO/Al_2O_3$ catalyst has been employed for over 50 years.[12–15] However, CO_2 conversion and methanol selectivity at low temperature and pressure still have room for improvement,[16–18] and the tendency for the conventional $Cu/ZnO/Al_2O_3$ catalyst to deactivate due to sintering also makes it necessary to further improve its stability, by searching for better support materials,[19–21] adding suitable promoters,[22–24] and changing the synthesis method,[25,26] all of which can lead to enhanced catalyst performance. In addition, the unique role of and interaction between the Cu and ZnO components[27–29] were also examined to improve our understanding of the CO_2 hydrogenation mechanism for the rather complex $Cu/ZnO/Al_2O_3$ catalyst system, but our understanding on its active site and reaction mechanism remains very limited.

There remain debates on the nature of the active site of the $Cu/ZnO/Al_2O_3$ catalyst, although the Cu/ZnO interface or the CuZn alloy has been generally recognized as the active site for methanol synthesis.[12,30–35] Despite intensive efforts, it remains difficult for experimental methods alone to provide a thorough understanding on the active site and reaction mechanism of the $Cu/ZnO/Al_2O_3$ catalyst for methanol synthesis. For instance, X-ray photoelectron

[a] *CAS Key Laboratory of Low-Carbon Conversion Science and Engineering, Shanghai Advanced Research Institute, Chinese Academy of Sciences, 100 Haike Road, Shanghai 201210, China. E-mail: gaopeng@sari.ac.cn, lisg@sari.ac.cn*
[b] *University of Chinese Academy of Sciences, Beijing 100049, China*
[c] *State Key Laboratory of Low Carbon Catalysis and Carbon Dioxide Utilization, Shanghai Advanced Research Institute, Chinese Academy of Sciences, Shanghai 201210, China*
[d] *School of Physical Science and Technology, ShanghaiTech University, Shanghai 201210, China*

† Electronic supplementary information (ESI) available. See DOI: https://doi.org/10.1039/d4cy00604f

spectroscopic (XPS) experiments have difficulty in clarifying the valence states of the Zn species due to its limited ability to distinguish the 2p peaks of the different Zn species.[30,36,37] In addition, introducing a reactive atmosphere can lead to significant changes in the already complex structure of the $Cu/ZnO/Al_2O_3$ catalyst, which makes it greatly challenging to elucidate the structure, properties, and reaction mechanism of the catalyst active site.[38–41]

The metal-oxide interface has unique electronic properties due to its strong interaction,[42–45] which has been proposed by experimental studies to promote the CO_2 hydrogenation reaction. Kattel *et al.* compared the activities of the oxide-on-metal ZnO/Cu and bimetallic ZnCu catalysts for CO_2 hydrogenation built from a single crystal model system, which illustrated the pivotal role of ZnO on the Cu surface and suggested the metal-oxide interface as the active site for methanol synthesis.[31] Wu *et al.* used the higher valent metal oxide ZrO_2 to construct the ZrO_2/Cu model catalyst, which greatly enhanced the reactivity of the Cu catalyst and showed excellent catalytic performance in methanol synthesis.[46] Recently, Liu *et al.* further proposed the interface of the oxygen-deficient ZnO and Cu to favour methanol synthesis from CO_2 hydrogenation through the HCOO pathway,[34] and ZnO_{1-x}/Cu catalysts with abundant oxygen vacancies prepared by Zhang *et al.* showed excellent methanol selectivity of above 90%.[47] These studies demonstrate the rational design of reverse oxide/metal configurations as efficient CO_2 hydrogenation catalysts and the importance of the oxygen vacancy in the CO_2 hydrogenation reaction.

Density functional theory (DFT) calculations can now provide important physical insights, and thus can potentially reduce the number of experimental trials. Previous computational studies suggest that methanol can be synthesized from CO_2 hydrogenation through the HCOO pathway, or *via* the reverse water gas shift (RWGS) reaction followed by CO hydrogenation, known as the RWGS + CO-hydro pathway.[31,34,42,48] Previous theoretical studies on the $Cu/ZnO/Al_2O_3$ catalyst for CO_2 hydrogenation to methanol mainly focused on the nature of the active site, as well as the morphology and metal coordination of the catalyst.[12,34,48–53] Catalyst models, including Cu-supported ZnO and ZnO-supported Cu, have been employed to simulate the ZnO/Cu interface, and the size and shape of the supported Cu cluster and ZnO cluster or nanoribbons were examined by several studies.[31,34,45,47,49,51–55] Some recent theoretical investigations examined the mechanism of CO_2 hydrogenation at the ZnO/Cu interface, which is generally modelled by placing ZnO clusters or nanoribbons on the Cu surface. Kattel *et al.*[31] and Liu *et al.*[34] constructed such ZnO/Cu catalyst models using different ZnO clusters or nanoribbons, and calculated the reaction pathway of CO_2 hydrogenation to methanol through the above two reaction pathways at the perfect or oxygen-deficient ZnO/Cu interface, but only focused on the interfacial site between the ZnO and the Cu(111) surface. It is worth noting that in these reverse oxide-on-metal catalyst models, the metal is modified by the reducible oxide, and there are metal, redox, and Brønsted and Lewis acid sites,[56] so the reaction mechanism can be more complex than that on the pure metal or pure oxide surface. To this end, DFT calculations can greatly improve our understanding on the properties of the active site of the $Cu/ZnO/Al_2O_3$ catalyst as well as the reaction mechanism for CO_2 hydrogenation especially when combined with results from various experimental characterization techniques.

In this work, extensive DFT calculations were performed to reveal the mechanisms of H_2 and CO_2 activation at the interface of the ZnO/Cu model catalyst during CO_2 hydrogenation. Our results show that the ZnO/Cu interface plays a vital role in H_2 dissociation, which provides H adsorbates for CO_2 hydrogenation. Hydrogen spillover from the Cu surface to the terminal O of the ZnO ribbons results in Brønsted acid and redox sites at the ZnO/Cu interface. The interfacial V_O site formed upon hydrogen spillover from Cu to ZnO facilitates both the direct dissociation of CO_2 and the formation of the HCOO intermediate by CO_2 hydrogenation. The size of the ZnO ribbon and the exposed Cu crystal plane have important effects on H_2 activation, which is relevant to the formation of interfacial V_O sites. Our work thus provides significant physical insights on the mechanisms of H_2 and CO_2 activation at the ZnO/Cu interface, which are crucial towards the rational design of more active Cu-based catalysts for CO_2 hydrogenation to methanol.

2 Computational methods

All periodic DFT calculations were carried out with the Vienna *ab initio* simulation package (VASP)[57,58] using the Perdew–Burke–Ernzerhof (PBE)[59] exchange–correlation functional and the projector-augmented wave (PAW) potentials.[60,61] An energy cutoff of 400 eV and a Gaussian smearing width of 0.05 eV were used. The electronic energy in the self-consistent field (SCF) iteration was set to 10^{-4} eV, and the forces on all unconstrained atoms were converged to 0.03 eV $Å^{-1}$. A vacuum space of 15 Å was used to separate adjacent slabs along the *Z* direction.

Recently, inverse ZnO/Cu catalyst models with ZnO clusters or nanoribbons supported on the Cu slab surface were constructed to simulate the ZnO/Cu surface.[31,34,49,55] Considering the ZnO overlayer observed in experiments of $Cu/ZnO/Al_2O_3$ catalysts,[34,62–64] catalyst models with ZnO ribbons are used in this work. The interface between Cu and ZnO was modelled by placing a layer of (3 × 3) ZnO(0001) ribbon on top of the three-layer (4 × 8) Cu(111) slab, the three-layer (3 × 5) Cu(100) slab, or the five-layer (3 × 4) Cu(211) slab. For comparison, interface models were also built by loading the smaller one-layer (2 × 3) ZnO(0001) ribbon on the above Cu surfaces. We use $W_y^x(z)$ to represent the six models, where *x*, *y*, and *z* refer to the number of ZnO layers, the number of columns of ZnO ribbons, and the Miller index of the Cu surface, respectively. For instance, Fig. 1(a) shows the catalyst model denoted by $W_3^1(111)$, where one layer of the three columns of ZnO ribbons is supported

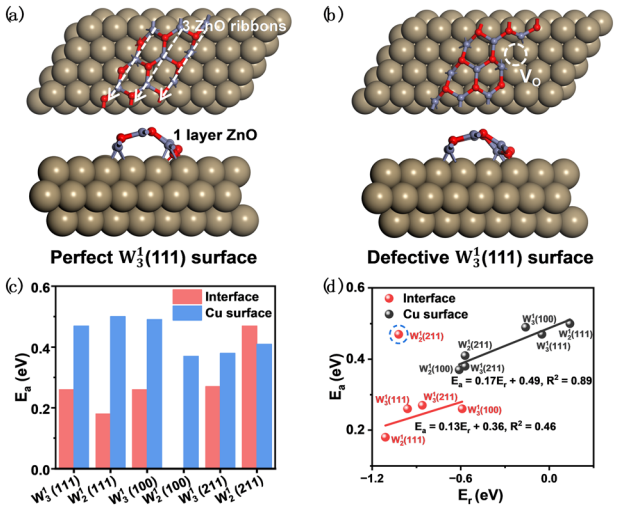

Fig. 1 Top and side views of (a) perfect and (b) defective W$_3^1$(111) surfaces; comparison of (c) the calculated energy barriers (E_a/eV); and (d) BEP relationship for H_2 dissociation at the ZnO/Cu interface and the Cu surface.

by the Cu(111) surface. Our calculations show that catalyst models with three Cu layers can give results as accurate as with five Cu layers including adsorption energies, reaction energies, and energy barriers as shown in Fig. 4, 5 and S1.† For the ZnO/Cu catalyst models containing ZnO ribbons employed in this work, the mismatch along the extended direction of the ZnO ribbons may result in some strain between these two components, and the misfit can be calculated using the following equation:

$$f = \frac{a_{\text{Cu slab}} - a_{\text{ZnO ribbon}}}{a_{\text{Cu slab}}}$$

where $a_{\text{Cu slab}}$ represents the lattice parameters of (4 × 8) Cu(111), (3 × 5) Cu(100), (3 × 4) Cu(211) slabs along the direction of the extended ZnO ribbons, and $a_{\text{ZnO ribbon}}$ represents the lattice parameter of ZnO(0001) along the interface region. We find that the misfits between the ZnO ribbon and Cu slab in the W$_3^1$(111), W$_2^1$(111), W$_3^1$(100), W$_2^1$(100), W$_3^1$(211), and W$_2^1$(211) catalyst models are 5.25%, 5.25%, 10.71%, 10.71%, 5.25%, and 5.25%, respectively, so only the misfits of the ZnO ribbon and Cu(100) slab are relatively large, and the resulting catalyst models may be less stable compared to the others. Thus, we focus our discussion on the computational results for the reasonably stable W$_3^1$(111), W$_2^1$(111), W$_3^1$(211), and W$_2^1$(211) catalyst models.

For W$_3^1$(111) and W$_2^1$(111), the Brillouin zone was sampled with a Monkhorst–Pack k-point grid mesh of (3 × 1 × 1), whereas for W$_3^1$(100) and W$_2^1$(100), it was sampled with that of (2 × 1 × 1); in these calculations, the bottom two atomic layers were fixed, whereas the top atomic layer and the adsorbed species were relaxed. For W$_3^1$(211) and W$_2^1$(211), the Brillouin zone was sampled with a Monkhorst–Pack k-point grid mesh of (1 × 2 × 1), and the bottom three atomic layers were fixed, whereas the top two atomic layers and the adsorbed species were relaxed. The k-points for the different ZnO/Cu catalyst models were generated using the VASPKIT program with the recommended KPT-resolved value of 0.04 2 × π/Å.[65]

The Hubbard U correction for the Zn atoms was included in our DFT calculations to treat the on-site Coulomb repulsion of their 3d electrons using an effective U value of 4.7 eV ($U_{\text{eff}} = U - J$) based on the previous work of Liu *et al.*[34] The climbing-image nudged elastic band (CI-NEB) method[66,67] and the improved dimer method (IDM)[68] were employed to locate the transition states, which were further verified by vibrational analysis showing one and only one imaginary mode. All structures were built and visualized using Materials Visualizer from Materials Studio.[69]

The formation energy of a V_O site ($\Delta E_{f,V_O,O_2}$) with respect to gas phase O_2 is defined as the reaction energy of the thermal desorption of molecular O_2:

$$\Delta E_{f,V_O,O_2} = E_{V_O\text{-surface}} - E_{\text{perfect}} + \frac{1}{2}E_{O_2}$$

In addition, the formation energy of a V_O site ($\Delta E_{f,V_O,H_2/H_2O}$) with respect to gas phase H_2/H_2O is defined as:

$$\Delta E_{f,V_O,H_2/H_2O} = E_{V_O\text{-surface}} - E_{\text{perfect}} - \frac{1}{2}E_{H_2} + \frac{1}{2}E_{H_2O}$$

where $E_{V_O\text{-surface}}$, E_{perfect}, E_{O_2}, E_{H_2} and E_{H_2O} denote the total energies of the defective surface, perfect surface, and gas phase O_2, H_2 and H_2O. The adsorption energy of an adsorbate A on the ZnO/Cu slab surface S is defined as:

$$E_{ad,A} = E_{\text{total}} - (E_{\text{slab}} + E_A)$$

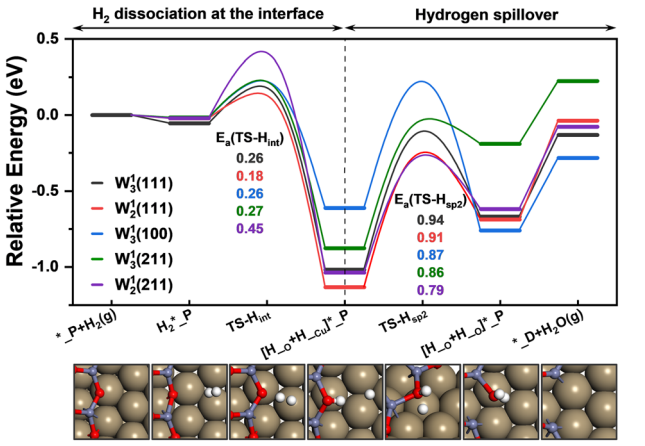

Fig. 2 Potential energy profiles for H_2 dissociation at the interface and the subsequent hydrogen spillover process with their energy barriers (E_a/eV) shown. The images display structures of the intermediates and transition states on the perfect W$_3^1$(111) surface. Brown: Cu, grayish blue: Zn, red: O, white: H.

where E_{total}, E_{slab}, and E_A are the total energies of the slab with the adsorbate, the clean slab, and the adsorbate as a free molecule, respectively.

3 Results and discussion

3.1 H_2 dissociation at the ZnO/Cu interface and the Cu surface

We first compare the dissociative adsorption of H_2 at the ZnO/Cu interface and the traditional Cu surface sites.[70] As shown in Fig. 1 and 2, unlike the homolytic dissociation of H_2 on the Cu surface (TS-H_{Cu}), the heterolytic dissociation of H_2 at the perfect ZnO/Cu(*_P) interface (TS-H_{int}) leads to two H adsorbates at the O and Cu sites, where one H atom ($H_{\_O}$*) is adsorbed at the terminal O site of ZnO resulting in a Brønsted acid site, and the other H atom ($H_{\_Cu}$*) is adsorbed on the Cu surface. For the perfect $W_3^1(111)$ surface, the O–H_A bond formed after H_2 dissociation has a length of 0.98 Å, while the other H atom is adsorbed at the three-fold hollow site surrounded by three Cu atoms. H_2 dissociation at this interfacial site has a lower energy barrier (E_a) of 0.26 eV than that on the Cu surface of 0.47 eV. In its transition state, the distance between H_A and H_B is 0.91 Å, similar to that on the Cu surface of 0.92 Å. H_2 dissociation on the Cu(100) and Cu(110) surfaces was also investigated by Higham *et al.*,[71] whose energy barriers were calculated to be 0.54 and 0.42 eV; these values are in good agreement with our results for the homolytic dissociation of H_2 on the Cu surfaces. Besides, our calculated energy barrier for the heterolytic dissociation of H_2 at the ZnO/Cu interface is comparable to 0.17 eV for the homolytic dissociation of H_2 at the Zn sites over the perfect Zn-terminated ZnO(0001) surface.[72] The energy barriers of H_2 dissociation on all studied ZnO/Cu catalyst models are compared in Fig. 1(c), and those at the interface are generally much lower than those on the Cu surfaces. In addition, H_2

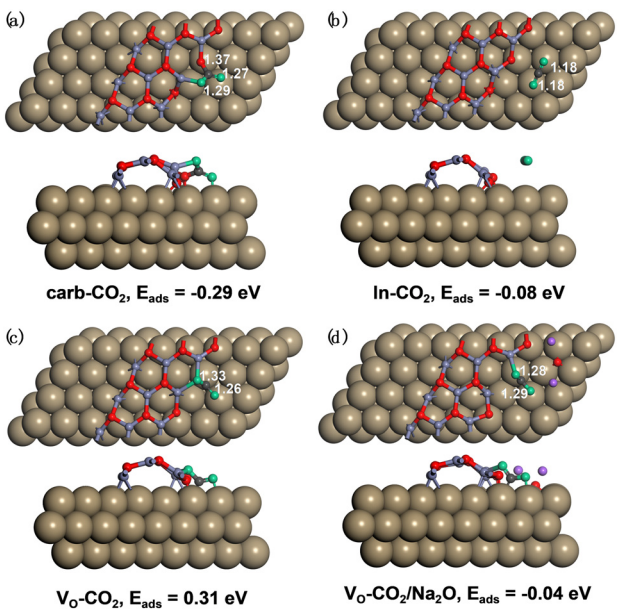

Fig. 3 Adsorption structures and adsorption energies (E_{ads}/eV) of (a) carb-CO_2^*, (b) In-CO_2^* on the perfect $W_3^1(111)$ surface, (c) V_O-CO_2^* on the defective $W_3^1(111)$ surface, and (d) V_O-CO_2^* in the presence of the Na promoter. Brown: Cu, greyish blue: Zn, red: O, dark grey: C, green: O in CO_2 molecules, purple: Na.

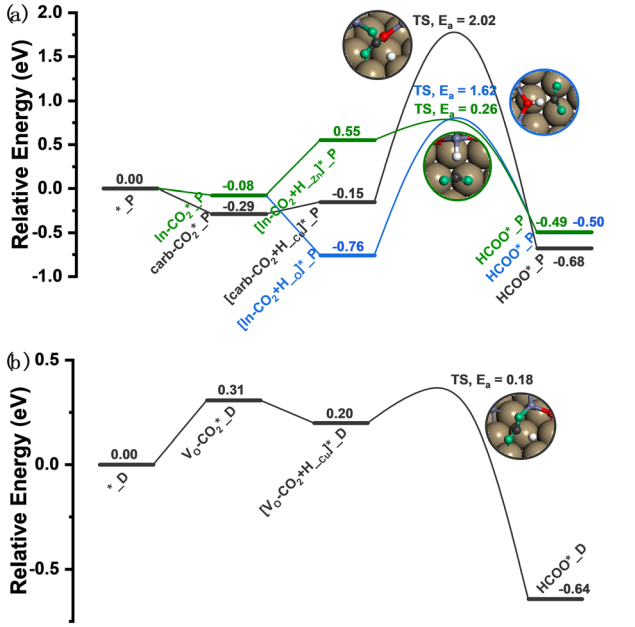

Fig. 4 Potential energy profiles for CO_2 hydrogenation to the HCOO* intermediate at the interface of the (a) perfect and (b) defective $W_3^1(111)$ surfaces. Structures of the transition states on the perfect and defective $W_3^1(111)$ surfaces are shown.

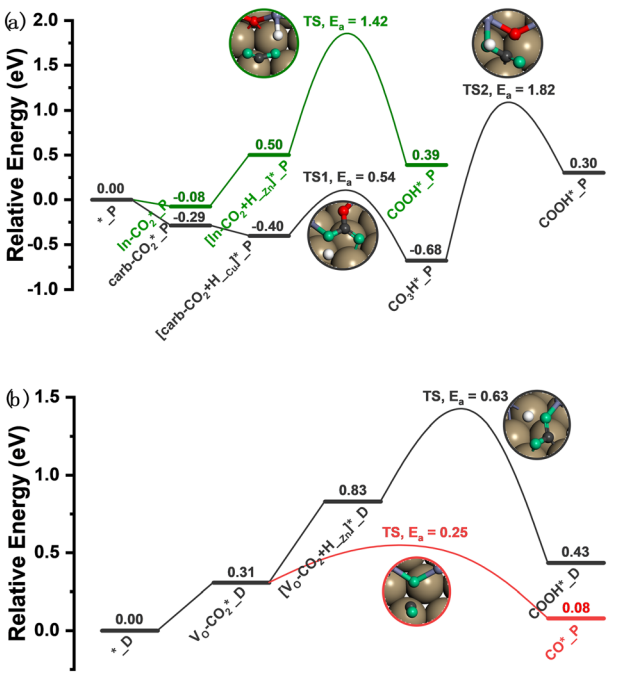

Fig. 5 Potential energy profiles for CO_2 direct and indirect dissociations at the interface of the (a) perfect and (b) defective $W_3^1(111)$ surfaces. Structures of the transition states on the perfect and defective $W_3^1(111)$ surfaces are shown.

dissociation at the interface is strongly exothermic, indicating that it is favoured both thermodynamically and kinetically. Further details in the calculated energy barriers and reaction energies (E_r) are given in Table S1.†

Fig. 1(d) further shows the Bell–Evans–Polanyi (BEP)[73–75] relationship between the energy barrier and the reaction energy for H_2 dissociation at the perfect ZnO/Cu interface and on the Cu surface. The BEP relationship for H_2 dissociation on the Cu surface shows a reasonably good linear fit with a coefficient of determination (COD) of R^2 = 0.89, which makes it possible to estimate the energy barrier of H_2 dissociation from its reaction energy on the Cu surface. However, the BEP relationship for H_2 dissociation at the perfect ZnO/Cu interface is more complex than linear, as indicated by the low COD of R^2 = 0.46 when a linear fit is attempted even by including only four catalyst models and excluding the perfect $W_2^1(211)$ interface, which is marked by the blue dashed circle and is clearly an outlier. Thus, although a roughly linear trend appears between the energy barrier and the reaction energy of H_2 dissociation at the interfacial sites of ZnO and different Cu crystal planes, the linearity is not nearly as good as that on the Cu surface.

3.2 Hydrogen spillover mechanism

To study the mechanism and effect of hydrogen spillover on oxygen vacancy formation, we then calculated the formation energy of oxygen vacancies ($\Delta E_{f,V_O,O_2}$) with respect to gas phase O_2 at the interfaces of the different ZnO/Cu catalyst models. For the perfect $W_3^1(111)$ interface model shown in Fig. 1(a), we find that the O sites from the rightmost ZnO ribbon are more likely to be hydrogenated to form oxygen vacancies due to their lower oxygen vacancy formation energies (with an average oxygen vacancy formation energy of 2.94 eV as listed in Table S2†) than those from the other two ZnO ribbons. For the other five catalyst models, the oxygen vacancy formation energies of the O sites from the rightmost ZnO ribbon are generally also lower, indicating the more likely location of oxygen vacancy formation at the ZnO/Cu interface. Thus, in our subsequent calculations, the defect site at the ZnO/Cu interface is chosen to be located at the O site from the rightmost ZnO ribbon.

Fig. 2 and Tables S1 and S3† show H_2 dissociation at the ZnO/Cu interface and on the Cu surface, leading to two hydrogen spillover mechanisms and oxygen vacancy formation at the interface. After H_2 dissociation at the interface, the H atom adsorbed on the Cu surface is further transferred to the Brønsted acid site (OH site) (TS-H_{sp2}), which is itself formed from H_2 dissociation. The energy barrier of this step is between 0.79 and 0.94 eV, and an adsorbed H_2O molecule is formed after the hydrogen spillover. Upon H_2O desorption, an oxygen vacancy site is formed leading to the defective ZnO/Cu surfaces (*_D).

In contrast, after H_2 dissociation on the Cu surface, an additional hydrogen spillover step is required to first form the aforementioned Brønsted acid site followed by the further formation of the oxygen vacancy site by another hydrogen spillover step. Over the perfect ZnO/Cu surfaces, after H_2 dissociation on the Cu surface, both H atoms are adsorbed on the hollow Cu sites. For the perfect $W_3^1(111)$ surface, the first H adsorbate diffuses from the Cu surface to the terminal O of ZnO to form a Brønsted acid site (TS-H_{sp1}) with an energy barrier of 0.74 eV and an exothermicity of −0.54 eV. Then, the second H atom also spills over from the Cu surface to the above Brønsted acid site to form an adsorbed H_2O molecule (TS-H_{sp2}), desorption of which results in an oxygen vacancy and the defective surface as shown in Fig. 1(b).

As discussed in the previous section, H_2 tends to dissociate at the ZnO/Cu interface. Nevertheless, the above-mentioned two hydrogen spillover processes are both likely to occur, so the ZnO/Cu interface can promote H_2 dissociation to form a Brønsted acid site, as well as the formation of a Brønsted acid site and an oxygen vacancy site after hydrogen spillover. As shown in Table S2,† the formation energies of an oxygen vacancy ($\Delta E_{f,V_O,H_2/H_2O}$) with respect to gas phase H_2/H_2O for the interfacial O atoms in ZnO are mostly negative, ranging from −0.28 to −0.04 eV, except for that in $W_3^1(211)$ of 0.18 eV, indicating that the formation of the interfacial V_O sites in these catalyst models are usually thermodynamically favorable. Under the actual reaction conditions, H_2O molecules, which are also products of CO_2 hydrogenation, are also present in the reaction atmosphere, so we also consider the possible dissociation of H_2O at the ZnO component to form Brønsted acid sites. As shown in Fig. S2 and Table S3,† H_2O dissociation at the ZnO component involves a rather low energy barrier of <0.30 eV, leading to the formation of two hydroxyl groups (Zn–OH). This indicates that H_2O produced during CO_2 hydrogenation may also promote the formation of Brønsted acid sites, and as the reaction proceeds, the ZnO component will likely undergo continuous hydrogenation and redox reactions, leading to dynamic structural changes.

3.3 CO_2 adsorption at the ZnO/Cu interface

CO_2 can potentially adsorb at the metal site or the oxygen vacancy site on the ZnO/Cu model catalyst. For the perfect and defective $W_3^1(111)$ surfaces, CO_2 can adsorb at the interfacial O site of ZnO on the perfect ZnO/Cu surface to form the carbonate configuration (carb-CO_2^*) as shown in Fig. 3(a), or physisorb in a linear CO_2^* configuration (ln-CO_2^*) as shown in Fig. 3(b), or chemisorb at the interfacial oxygen vacancy site on the defective $W_3^1(111)$ surface to form the bent CO_2^* configuration (V_O-CO_2^*) as shown in Fig. 3(c). The different CO_2 adsorption structures on the different ZnO/Cu catalyst models are shown in Fig. S3 and S4.†

For the perfect $W_3^1(111)$ surface without an oxygen vacancy site at the interface, CO_2 can combine with a terminal O atom of ZnO to form the carb-CO_2^*, where the C–O bond lengths in the adsorbed CO_2 are elongated to 1.27 and 1.29 Å with the formation of a new C–O bond of 1.37 Å. During the adsorption, the original Zn–O bond is broken, and this Zn

atom binds one O atom in the adsorbed CO_2, while the other O atom in CO_2 binds the surface Cu atom. CO_2 can also physisorb in the ln-CO_2^* at the perfect ZnO/Cu interface, which undergoes little changes from the free CO_2 molecule. For the defective $W_3^1(111)$ surface with an oxygen vacancy site at the interface, CO_2 can chemisorb in the V_O-CO_2^*, which undergoes significant deformation compared to the free CO_2 molecule, resulting in two C–O bonds of 1.26 and 1.33 Å and an O–C–O bond angle of 120.5°. In the V_O-CO_2^*, the oxygen vacancy is essentially occupied by one O atom in CO_2, while the other O and the C atoms bind different surface Cu atoms.

As shown in Tables 1 and S4,† after CO_2 adsorption in the carb-CO_2^* on the perfect $W_3^1(111)$ surface, the Bader charges of the Cu and Zn atoms bound to the adsorbate increase by 0.17 and 0.11 |e|, respectively, while the Bader charges of the O atoms in the adsorbate decrease by 0.09 |e|. Furthermore, after CO_2 adsorption in the V_O-CO_2^* on the defective $W_3^1(111)$ surface, the Bader charges of the two Cu atoms around the adsorbate increase by 0.22 and 0.13 |e|, whereas the Bader charges of the two Zn atoms around the adsorbate also increase by 0.29 and 0.23 |e|.

In addition, as shown in Table S5,† the negative charge on ZnO over the defective surface is significantly lower than that over the perfect surface, so the presence of the oxygen vacancy sites greatly reduces the number of electrons transferred from Cu to ZnO. We note that an opposite direction of charge transfer was predicted by Heenemann *et al.* for the ZnO-supported Cu nanoparticle models.[76] When CO_2 is adsorbed on both the perfect and defective surfaces, CO_2 acquires some electrons, and that in the V_O-CO_2^* obtains about one electron, which is significantly more than that in the carb-CO_2^* of 0.17 electrons on average. For example, after CO_2 adsorption on the defective $W_3^1(111)$ surface, the CO_2 adsorbate obtains 0.99 |e|, and the Bader charges of the other adsorbed CO_2 are shown in Table S5.† This suggests that the presence of the oxygen vacancy site can significantly promote electron transfer from the defective surface to the CO_2 adsorbate. Thus, the V_O-CO_2^* may be more likely hydrogenated to the HCOO intermediate, because it carries more negative charge and is partially reduced upon the formation of the oxygen vacancy.[77,78]

Table 1 Calculated Bader charges and corresponding changes for the Cu, Zn and O atoms around the adsorbate before and after CO_2 adsorption on the perfect surface (*_P) and defective surface (*_D). Q2 and Q4 represent the positive charges of Cu, Zn atoms and the negative charges of O atoms around the adsorbed CO_2 molecule, Q1 and Q3 represent the corresponding charges of these atoms before CO_2 adsorption

$W_3^1(111)$ surface	Q/|e|	Cu	Zn	O
*_P	Q1 (*_P)	0.00	1.08	−1.08
	Q2 (carb-CO_2^*_P)	0.17	1.19	−1.17
	ΔQ1 (= Q2 − Q1)	0.17	0.11	−0.09
*_D	Q3 (*_D)	−0.03/−0.05	0.83/0.80	—
	Q4 (V_O-CO_2^*_D)	0.19/0.08	1.12/1.03	—
	ΔQ2 (= Q4 − Q3)	0.22/0.13	0.29/0.23	—

It is worth noting that although the V_O-CO_2^* obtains more electrons than the carb-CO_2^*, the adsorption energy of the V_O-CO_2^* is significantly less negative than that of the carb-CO_2^*. As shown in Table S6,† the adsorption energy of the carb-CO_2^* on the perfect $W_3^1(111)$ surface is −0.29 eV, which is much more negative than that of V_O-CO_2^* on the defective $W_3^1(111)$ surface of 0.31 eV. Reichenbach *et al.* also reported a similar observation that adsorption of the activated CO_2 molecule on the ZnO cluster models with different oxidation states for Zn is relatively unstable with CO_2 adsorption energies of 0.28–0.66 eV.[49] We conjecture that introducing the Na_2O promoter may further enhance the adsorption of the V_O-CO_2^*, and as shown in Fig. 3(d), our calculations show that adding Na_2O can indeed change its adsorption energy from 0.31 to −0.04 eV, thus leading to stronger adsorption. Besides, although the carbonate adsorption structures are much stable at the ZnO/Cu interface compared to the V_O-CO_2^*, recent computational works suggest that the carbonate species, which is easy to form and stable, will block the active sites of the ZnO surface;[72,79] the role of the carbonate will be further discussed in the next section.

In summary, the CO_2 adsorbates in both the carb-CO_2^* and the V_O-CO_2^* appear to be activated considering the decrease in the C–O–C angle and the increase of the C–O bond length, compared with that in the ln-CO_2^*. However, the absence or presence of the oxygen vacancy at the ZnO/Cu interface shows a distinct effect on the stability of the carb-CO_2^* and the V_O-CO_2^*, in which the activated carb-CO_2^* is more stable than the activated V_O-CO_2^* at the ZnO/Cu interface. Although the carb-CO_2^* is thermodynamically more stable and the V_O-CO_2^* has an endothermic adsorption energy, the oxygen vacancy site promotes the charge transfer in the latter leading to the accumulation of more electrons on the CO_2 adsorbate, which may facilitate its further conversion.

3.4 HCOO formation at the ZnO/Cu interface

It is generally believed that CO_2 can be hydrogenated to methanol *via* the formate (HCOO) pathway,[77,80–83] where H can either come from direct H_2 dissociation or from the Brønsted acid site resulting from hydrogen spillover as discussed in the earlier section. We thus examined CO_2 adsorption at the ZnO/Cu interface, and its further hydrogenation to the HCOO intermediate.

As shown in Table S7,† in the absence of an oxygen vacancy site at the ZnO/Cu interface, hydrogenation of the carb-CO_2^* to the HCOO intermediate needs to overcome a very high energy barrier of >2.00 eV, and the energy barrier for the hydrogenation of the ln-CO_2^* by H* from the Brønsted acid site to the HCOO intermediate remains substantial at 1.42–1.62 eV, whereas the energy barrier of the hydrogenation of the ln-CO_2^* by H* adsorbed on the Zn site is the lowest at only 0.24–0.34 eV. At the perfect $W_3^1(111)$ interface, the detailed reaction pathway for the hydrogenation of the

carb-CO_2^* and ln-CO_2^* adsorbates to form the HCOO* is shown in Fig. 4(a). The carb-CO_2^* can react with the H* adsorbed at the hollow Cu site with a very high energy barrier of 2.02 eV and an exothermicity of −0.53 eV, where the dissociated O atom binds the Zn site, confirming the inactivity of the carbonate at the ZnO/Cu interface for methanol synthesis, similar to that on the ZnO surface.[72,79] The ln-CO_2^* can react with the H* adsorbed at the O site with a substantial energy barrier of 1.62 eV and an endothermicity of 0.26 eV. The same reaction step of CO_2 hydrogenation to HCOO* through H atoms in the Brønsted acid site was calculated by Liu *et al.* to have a lower energy barrier of 1.15 eV,[34] which is likely due to the adsorption of the reactant CO_2 molecule at the Cu sites near the interface, different from the physisorbed CO_2 in our work. Furthermore, the ln-CO_2^* can also react with the H* adsorbed at the Zn site to form the HCOO* with a very low energy barrier of 0.26 eV and an exothermicity of −1.05 eV. The significant difference in the reaction barrier and reaction energy for the hydrogenation of the ln-CO_2^* by the H_O* and H_Zn* can be attributed to the different affinity of the H* adsorbate to the O and Zn sites. This can be inferred from the rather close effective energy barriers ($E_{a,eff}$) for the hydrogenation of the ln-CO_2^* to the HCOO* in these two pathways, which are 0.94 and 0.88 eV involving the H_O* and H_Zn*, respectively.

In the presence of an oxygen vacancy site at the interface, hydrogenation of the V_O-CO_2^* to form the HCOO* only needs to overcome a very low energy barrier of 0.18–0.30 eV, indicating that CO_2 can be easily converted into the HCOO* intermediate at the oxygen vacancy site. The detailed energy barriers and reaction energies are listed in Table S7,† and for the defective $W_3^1(111)$ surface, the detailed reaction pathway for the hydrogenation of the V_O-CO_2^* adsorbed at the interface to form the HCOO* is shown in Fig. 4(b). The V_O-CO_2^* can react with the H* adsorbed at the hollow Cu site to form the HCOO* with a very low energy barrier of only 0.18 eV and an exothermicity of −0.84 eV, where the C–H distance shrinks from 2.54 Å in the initial state to 1.66 Å in the transition state, and the resulting C–O bond lengths in the HCOO* are 1.25 and 1.29 Å. Over other catalyst models such as Cu supported ZnO clusters, similar energy barriers of no more than 0.30 eV were predicted for hydrogenation to HCOO* of the bent CO_2 adsorbates with one O atom adsorbed at the Zn site,[31,51] comparable with that on the ZnO surface of 0.11 eV,[72,79] while hydrogenation to HCOO* of the linear CO_2 adsorbates with one O atom adsorbed at the Zn sites needs to overcome a slightly higher energy barrier[49] of about 0.60 eV. Thus, these catalytically active sites all exhibit higher activity for HCOO* formation than the Cu surface.[71,81]

3.5 CO_2 dissociation at the ZnO/Cu interface

Methanol may also form from hydrogenation of the CO intermediate, which is produced from the reverse water gas shift (RWGS) reaction. CO can form either by the direct dissociation of the adsorbed CO_2^* to CO* and O*, or by the indirect dissociation pathway *via* the carboxylic acid (COOH*) intermediate, which can further dissociate into CO* and OH*. We examined the direct dissociation and the COOH* pathways from the different CO_2 adsorption structures, and the detailed energy barriers and reaction energies are listed in Tables S8 and S9.† In the absence of an oxygen vacancy on the surface, the ln-CO_2^* can be directly hydrogenated to the COOH*, while the carb-CO_2^* must be first hydrogenated into the bicarbonate (CO_3H*) intermediate prior to its further conversion to the COOH*. On the other hand, in the presence of an oxygen vacancy on the surface, the V_O-CO_2^* can be converted into CO by both the direct and indirect pathways.

For the perfect $W_3^1(111)$ surface, the detailed reaction pathways for the hydrogenation of the carb-CO_2^* and ln-CO_2^* to form the COOH* are shown in Fig. 5(a). The O in the carb-CO_2^* can be first hydrogenated with the H* adsorbed on the Cu site to form the CO_3H* species with a relatively low energy barrier of 0.54 eV and an exothermicity of −0.27 eV. However, breaking the C–O bond in the CO_3H* to form the COOH* must overcome a very high energy barrier of 1.82 eV, indicating that converting the carb-O_2^* to CO* by hydrogenation is difficult. Similarly, our calculations show that it also seems difficult for hydrogenation of the ln-CO_2^* by an H atom adsorbed at the Zn site to form the COOH* to occur due to the rather high energy barrier of 1.42 eV. Therefore, in the absence of an oxygen vacancy on the surface, the adsorbed CO_2 molecule can only be converted into CO by the indirect pathway, which is expected to be slow due to the high energy barrier, and similar conclusions can be drawn for the indirect dissociation of CO_2 at the ZnO/Cu interface for the other studied catalyst models. This suggests that the perfect ZnO/Cu interface is rather inactive for the conversion of CO_2 into either the HCOO or COOH intermediate, so the absence of oxygen vacancy sites may lead to low CO_2 activity.

In the presence of an oxygen vacancy at the interface, our calculations using the different catalyst models show that CO_2 dissociation to form CO easily occurs. For the defective $W_3^1(111)$ surface, Fig. 5(b) shows the detailed potential energy diagrams for the direct dissociation of the adsorbed V_O-CO_2^* at the interface and for its hydrogenation to form the COOH* intermediate. As indicated by the red line in this figure, the V_O-CO_2^* can directly dissociate at the oxygen vacancy site to yield CO* and O* occupying the oxygen vacancy site with a very low energy barrier of 0.25 eV and an exothermicity of −0.23 eV. In this reaction, one O atom in the V_O-CO_2^* binds two Zn atoms in the ZnO ribbon, and the C–O distance in the transition state is 1.74 Å. The resulting CO molecule is adsorbed at the Cu site with C–Cu and C–O bond lengths of 1.85 and 1.16 Å, respectively. There is a lack of theoretical investigation on direct dissociation of CO_2, especially on the inverse ZnO/Cu catalyst models. Our results show that the V_O sites at the interface favor this process with an energy barrier of 0.25 eV, which is much lower than those of about 0.60–0.79 eV on the CuZn alloy.[31,48] In addition, the V_O-CO_2^* can

also be hydrogenated by the H* adsorbed at the Zn site to form the COOH* with an exothermicity of −0.39 eV, and its energy barrier of 0.63 eV is significantly higher than that to the HCOO* of 0.18 eV likely due to the oxophilicity of the Zn site. Thus, based on the above analysis, oxygen vacancy formation is not only conducive to CO_2 hydrogenation to form the HCOO* intermediate, but can also promote the direct dissociation of CO_2 to form CO, which is crucial for the subsequent CO hydrogenation reaction pathway. Furthermore, our calculations show that the presence of oxygen vacancies in ZnO is mostly to increase CO_2 reactivity, whereas its effect on the product selectivity may be rather limited.

3.6 Effects of the ZnO size and Cu crystal plane on H_2 activation

In our simulations, we considered catalyst models with different sizes of ZnO ribbons loaded on the Cu surface, including ZnO ribbons of three and two columns with all Zn atoms exposed. For ZnO ribbons of different sizes loaded on the Cu(111) surface, namely, the $W_3^1(111)$ and $W_2^1(111)$ surfaces, we further compared the energy barriers of H_2 dissociation, hydrogen spillover, CO_2 hydrogenation, and dissociation. As shown in Fig. 6(a), ZnO size is shown to mainly influence H_2 dissociation and hydrogen spillover during CO_2 hydrogenation. When decreasing the ZnO size, the energy barrier of H_2 dissociation at the ZnO/Cu interface slightly decreases from 0.26 to 0.18 eV, but that on the Cu surface slightly increases, indicating that a better exposure of the Zn atoms may benefit H_2 dissociation at the ZnO/Cu interface. In addition, for oxygen vacancy formation, the energy barrier of the first hydrogen spillover step decreases from 0.74 to 0.50 eV, while that of the second hydrogen spillover step to form an H_2O molecule also slightly decreases. Thus, reducing the ZnO size is also conducive to the occurrence of hydrogen spillover.

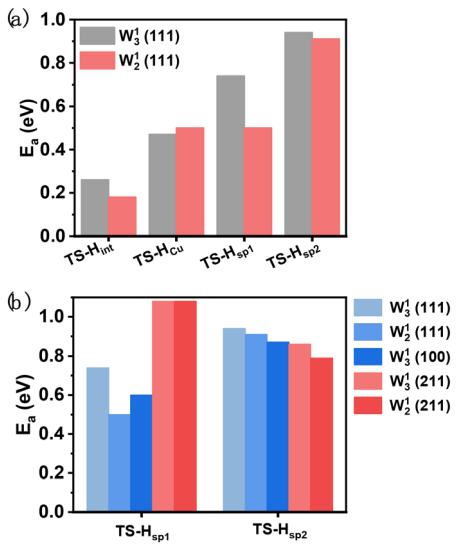

Fig. 6 (a) Comparison of the energy barriers of H_2 dissociation at the interface, Cu surface, and two hydrogen spillover processes on the $W_3^1(111)$ and $W_2^1(111)$ surfaces. (b) Comparison of energy barriers of the two hydrogen spillover processes at the interface of ZnO and different Cu crystal planes.

Using model catalysts with well-defined structures, such as specific metal surfaces,[12,51,84,85] may simplify the mechanistic investigation of complex catalysts. We thus also inspected the influence of the Cu crystal plane at the ZnO/Cu interface on the CO_2 hydrogenation reaction. As shown in Fig. 6(b), we find that at the interface between the Cu(211) facet and ZnO, the energy barrier of the first hydrogen spillover step is significantly higher, while that of the second hydrogen spillover step is slightly lower than those for the other studied Cu crystal facets. This indicates that to some extent, interfaces formed on the Cu(211) facet is less favourable for spillover of the H adsorbates formed by H_2 dissociation on the Cu surface, leading to less efficient formation of the Brønsted acid site (OH site).

3.7 Discussion

At present, our theoretical understanding on the ZnO/Cu interface for CO_2 hydrogenation to methanol remains lacking, and based on previous experimental and theoretical studies, we constructed a series of catalyst models with ZnO ribbons of different sizes loaded on different Cu crystal planes and examined the influence of the ZnO/Cu interfacial structure on the CO_2 hydrogenation reaction. Previously, Kattel *et al.* compared the activities of the ZnCu and ZnO/Cu model catalysts for methanol synthesis from CO_2 hydrogenation, and their DFT calculations on the ZnCu(211) and ZnO/Cu(111) surfaces identified the formate pathway and the RWGS + CO-hydro pathway for methanol synthesis from CO_2.[31] In this work, besides the Cu(111) facet, we also examined interfaces formed between ZnO ribbons and the slightly less stable Cu(211) and Cu(100) facets.[86] In addition, their studies suggest that O* formed by CO_2^* dissociation accumulates at the Zn sites on the ZnCu(211) surface, and hydrogenation of the resulting ZnO is hindered due to the relatively high energy barrier of 1.21 eV. Our calculations show that hydrogenation of the terminal O at the ZnO/Cu(211) interface to form the Zn-OH species also incurs a relatively high energy barrier of 1.08 eV, which is significantly higher than our other studied catalyst models. This suggests that the Cu(211) facet is less favourable for spillover of the H adsorbate at the ZnO/Cu interface. Furthermore, our results show more favourable CO_2 hydrogenation to the HCOO* than that to the COOH*, consistent with the theoretical studies of Kattel *et al.*[31] and Xiong *et al.*[51] using ZnO cluster models of the ZnO/Cu(111), ZnO/Cu(110), and ZnO/Cu(100) surfaces.

Recent experimental studies showed that the reverse ZnO/Cu model catalyst prepared by atomic layer deposition exhibits excellent performance for CO_2 hydrogenation to methanol, which is much higher than that using the Cu catalyst itself.[34] *In situ* X-ray absorption spectroscopy (XAS) further showed that the Zn species in

the highly active catalyst are present as oxygen-deficient ZnO aggregates. To elucidate the promotional effect of the Zn species on the Cu-based catalysts, theoretical calculations were performed to show that the oxygen-deficient ZnO_{1-x}/Cu(111) interface has high activity for methanol formation from CO_2 hydrogenation through the formate pathway, while indirect CO_2 dissociation incurs a relatively high energy barrier. In addition to the above-mentioned indirect CO_2 dissociation pathway, we also considered direct CO_2 dissociation at the defective ZnO/Cu interface. Our calculations show that the direct dissociation of the V_O-CO_2^* has the same low energy barrier as its hydrogenation to form the HCOO* intermediate. Thus, the defective ZnO/Cu interface can be expected to have rather similar reactivity to the ZnCu(211) surface for the competition between the direct dissociation and hydrogenation of CO_2.[31,48] HCOO*, the key reaction intermediate for methanol synthesis from CO_2 hydrogenation, can also be easily formed at the ZnO/Cu interface. With the accumulation of CO in the gas phase, it may undergo further hydrogenation to give methanol. However, previous isotope-labelling studies show that methanol is formed from the hydrogenation of CO_2 rather than CO,[82,87–89] whereas CO is regarded as a mere reducing agent. As Shi *et al.* reported,[90] under different H_2, CO, CO_2 pressure conditions, structures of the ZnO/Cu catalyst undergo dynamic changes, and CO can even reduce the Zn species. Furthermore, the HCO* species, which is involved in the CO hydrogenation route, are demonstrated as an unstable adsorbate, as the hydrogenation of HCO* usually incurs a higher energy barrier than the reverse reaction of CO* hydrogenation to HCO*. Many of the aforementioned studies reached the conclusion that the HCO* species should quickly dissociate to CO* and H* using quite different ZnO/Cu catalyst models, including the ZnO/Cu interface, ZnCu alloy, and pure Cu surfaces.[12,48,49,80,81,90–92] Besides, Liu *et al.* reported that CO_2 hydrogenation to methanol at the stoichiometric ZnO/Cu(111) interface through the H adatom strongly adsorbed at the edge oxygen site encounters rather high energy barriers. Although we find hydrogenation of the ln-CO_2* to the HCOO* by the weakly adsorbed $H_{\_Zn}$* to incur a very low energy barrier, the effective energy barrier for CO_2 hydrogenation by the $H_{\_Zn}$* is still quite high. Furthermore, our study shows that CO_2 can also adsorb on the perfect ZnO/Cu surface to form a carbonate species, although hydrogenation of this carbonate configuration is rather difficult, suggesting that the carbonate species is likely just a spectator.

Conclusions

In this study, we performed a systematic study on the effect of the interfacial structure of the ZnO/Cu catalysts for methanol synthesis from CO_2 hydrogenation using the reverse oxide-metal catalyst models with different sizes of ZnO ribbons loaded on different Cu crystal planes. The interfacial oxygen vacancy (V_O) sites on the ZnO/Cu model catalysts, formed by H_2 dissociation and subsequent hydrogen spillover at the ZnO/Cu interface, were found to be the effective active site for CO_2 activation and hydrogenation. Our main observations are the following:

(1) The formation of interfacial V_O sites from H_2 dissociation and hydrogen spillover is investigated. Our results show that H_2 molecules tend to dissociate at the ZnO/Cu interface with lower energy barriers instead of the Cu surface, and hydrogen spillover from Cu surfaces to the terminal O atoms of the ZnO occurs with moderate energy barriers to form V_O sites. These processes are kinetically favorable on most of the catalyst models with different sizes of ZnO ribbons and Cu crystal planes, consistent with the experimental observation of the promotion of methanol production by oxygen-deficient ZnO at the interface.

(2) Studies on the further conversion of the CO_2 adsorbates at the ZnO/Cu interface, including the hydrogenation, indirect, and direct dissociation, indicate that the interfacial V_O site accelerates the hydrogenation of the V_O-CO_2^* through the HCOO* pathway as well as the direct dissociation of CO_2, whereas the carbonate adsorption structure may act as a spectator. Thus, the ZnO/Cu interface containing V_O sites promotes the formation of the HCOO* intermediates and CO, similar to the CuZn alloy in previous studies.

(3) Catalyst models with smaller ZnO ribbons are more conducive to the formation of the interfacial V_O active site due to the lower reaction barrier of interfacial H_2 dissociation and hydrogen spillover from the Cu surface to the ZnO ribbon. However, the presence of the Cu(211) facet disfavours the first hydrogen spillover step during the formation of the Brønsted acid site, which may result in a lower coverage of the interfacial V_O site.

Our work reveals the mechanism of oxygen vacancy formation at the ZnO/Cu interface, and demonstrates the promotion of CO_2 activation and reaction at the ZnO/Cu interface, thus providing significant insights into the crucial role of ZnO/Cu interface sites in the CO_2 hydrogenation reaction.

Data availability

The data supporting this article have been included as part of the ESI.†

Conflicts of interest

There are no conflicts to declare.

Acknowledgements

This work was supported by the National Natural Science Foundation of China (22293023, 22172188, 22172189, 22293025), CAS Youth Interdisciplinary Team, Program of Shanghai Academic Research Leader (22XD1424100), and

Science and Technology Commission of Shanghai Municipality (23YF1453400, 23ZR1481700).

References

1 C. F. Shih, T. Zhang, J. Li and C. Bai, *Joule*, 2018, **2**, 1925–1949.
2 D. A. Lashof and D. R. Ahuja, *Nature*, 1990, **344**, 529–531.
3 P. Friedlingstein, R. M. Andrew, J. Rogelj, G. P. Peters, J. G. Canadell, R. Knutti, G. Luderer, M. R. Raupach, M. Schaeffer, D. P. van Vuuren and C. Le Quere, *Nat. Geosci.*, 2014, **7**, 709–715.
4 A. G. Olabi and M. A. Abdelkareem, *Renewable Sustainable Energy Rev.*, 2022, **158**, 112111.
5 J. F. D. Tapia, J. Y. Lee, R. E. H. Ooi, D. C. Y. Foo and R. R. Tan, *Sustain. Prod. Consum.*, 2018, **13**, 1–15.
6 K. Jiang, P. Ashworth, S. Y. Zhang, X. Liang, Y. Sun and D. Angus, *Renewable Sustainable Energy Rev.*, 2020, **119**, 109601.
7 S. Y. Chen, J. F. Liu, Q. Zhang, F. Teng and B. C. McLellan, *Renewable Sustainable Energy Rev.*, 2022, **167**, 112537.
8 R. P. Ye, J. Ding, W. Gong, M. D. Argyle, Q. Zhong, Y. Wang, C. K. Russell, Z. Xu, A. G. Russell, Q. Li, M. Fan and Y. G. Yao, *Nat. Commun.*, 2019, **10**, 5698.
9 S. Kar, A. Goeppert and G. K. S. Prakash, *Acc. Chem. Res.*, 2019, **52**, 2892–2903.
10 J. Zhong, X. Yang, Z. Wu, B. Liang, Y. Huang and T. Zhang, *Chem. Soc. Rev.*, 2020, **49**, 1385–1413.
11 S.-T. Bai, G. De Smet, Y. Liao, R. Sun, C. Zhou, M. Beller, B. U. W. Maes and B. F. Sels, *Chem. Soc. Rev.*, 2021, **50**, 4259–4298.
12 M. Behrens, F. Studt, I. Kasatkin, S. Kuhl, M. Havecker, F. Abild-Pedersen, S. Zander, F. Girgsdies, P. Kurr, B. L. Kniep, M. Tovar, R. W. Fischer, J. K. Norskov and R. Schlogl, *Science*, 2012, **336**, 893–897.
13 A. Alvarez, A. Bansode, A. Urakawa, A. V. Bavykina, T. A. Wezendonk, M. Makkee, J. Gascon and F. Kapteijn, *Chem. Rev.*, 2017, **117**, 9804–9838.
14 X. Jiang, X. Nie, X. Guo, C. Song and J. G. Chen, *Chem. Rev.*, 2020, **120**, 7984–8034.
15 A. Beck, M. A. Newton, L. G. A. van de Water and J. A. van Bokhoven, *Chem. Rev.*, 2024, **124**, 4543–4678.
16 Z. Chen, J. Wen, Y. Zeng, M. Li, Y. Tian, F. Yang, M. M.-J. Li, P. Chen, H. Huang, D. Ye and L. Chen, *Appl. Catal., B*, 2024, **340**, 123192.
17 J. Wang, Y. Song, J. Li, F. Liu, J. Wang, J. Lv, S. Wang, M. Li, X. Bao and X. Ma, *Appl. Catal., A*, 2024, **674**, 119618.
18 Y. Xu, Z. Gao, Y. Xu, X. Qin, X. Tang, Z. Xie, J. Zhang, C. Song, S. Yao, W. Zhou, D. Ma and L. Lin, *Appl. Catal., B*, 2024, **344**, 123656.
19 J. Zhu, D. Ciolca, L. Liu, A. Parastaev, N. Kosinov and E. J. M. Hensen, *ACS Catal.*, 2021, **11**, 4880–4892.
20 Y. Ou, T. Zhang, L. Lv, W. Tang and S. Tang, *Colloids Surf., A*, 2023, **676**, 132167.
21 C. Han, L. Qin, P. Wang, H. Zhang, Y. Gao, M. Zhu, S. Wang and J. Li, *Fuel*, 2024, **357**, 129945.
22 T. Qi, W. Li, H. Li, K. Ji, S. Chen and Y. Zhang, *Mol. Catal.*, 2021, **509**, 111641.
23 R. Dalebout, L. Barberis, N. L. Visser, J. E. S. van der Hoeven, A. M. J. van der Eerden, J. A. Stewart, F. Meirer, K. P. de Jong and P. E. de Jongh, *ChemCatChem*, 2022, **14**, e202200451.
24 F. Chen, W. Gao, K. Wang, C. Wang, X. Wu, N. Liu, X. Guo, Y. He, P. Zhang, G. Yang and N. Tsubaki, *Fuel*, 2022, **315**, 123272.
25 B. Hu, Y. Yin, Z. Zhong, D. Wu, G. Liu and X. Hong, *Catal. Sci. Technol.*, 2019, **9**, 2673–2681.
26 Y. Xu, Z. Gao, L. Peng, K. Liu, Y. Yang, R. Qiu, S. Yang, C. Wu, J. Jiang, Y. Wang, W. Tan, H. Wang and J. Li, *J. Catal.*, 2022, **414**, 236–244.
27 R. M. Palomino, P. J. Ramírez, Z. Liu, R. Hamlyn, I. Waluyo, M. Mahapatra, I. Orozco, A. Hunt, J. P. Simonovis, S. D. Senanayake and J. A. Rodriguez, *J. Phys. Chem. B*, 2017, **122**, 794–800.
28 A. Arandia, J. Yim, H. Warraich, E. Leppäkangas, R. Bes, A. Lempelto, L. Gell, H. Jiang, K. Meinander, T. Viinikainen, S. Huotari, K. Honkala and R. L. Puurunen, *Appl. Catal., B*, 2023, **321**, 122046.
29 C. Li, K. Chen, X. Wang, N. Xue and H. Yang, *Acta Phys.-Chim. Sin.*, 2020, **37**, 2009101.
30 S. Kuld, M. Thorhauge, H. Falsig, C. F. Elkjaer, S. Helveg, I. Chorkendorff and J. Sehested, *Science*, 2016, **352**, 969–974.
31 S. Kattel, P. J. Ramirez, J. G. Chen, J. A. Rodriguez and P. Liu, *Science*, 2017, **355**, 1296–1299.
32 J. Nakamura, T. Fujitani, S. Kuld, S. Helveg, I. Chorkendorff and J. Sehested, *Science*, 2017, **357**, eaan8074.
33 R. Dalebout, L. Barberis, G. Totarella, S. J. Turner, C. La Fontaine, F. M. F. de Groot, X. Carrier, A. M. J. van der Eerden, F. Meirer and P. E. de Jongh, *ACS Catal.*, 2022, **12**, 6628–6639.
34 X. Liu, J. Luo, H. Wang, L. Huang, S. Wang, S. Li, Z. Sun, F. Sun, Z. Jiang, S. Wei, W. X. Li and J. Lu, *Angew. Chem., Int. Ed.*, 2022, **61**, e202202330.
35 X. Liu, H. Wang and J. Lu, *J. Catal.*, 2024, **436**, 115561.
36 P. Amann, B. Klotzer, D. Degerman, N. Kopfle, T. Gotsch, P. Lomker, C. Rameshan, K. Ploner, D. Bikaljevic, H. Y. Wang, M. Soldemo, M. Shipilin, C. M. Goodwin, J. Gladh, J. H. Stenlid, M. Borner, C. Schlueter and A. Nilsson, *Science*, 2022, **376**, 603–608.
37 D. Laudenschleger, H. Ruland and M. Muhler, *Nat. Commun.*, 2020, **11**, 3898.
38 W. Tu, P. Ren, Y. Li, Y. Yang, Y. Tian, Z. Zhang, M. Zhu, Y. C. Chin, J. Gong and Y. F. Han, *J. Am. Chem. Soc.*, 2023, **145**, 8751–8756.
39 L. Xu, K. G. Papanikolaou, B. A. J. Lechner, L. Je, G. A. Somorjai, M. Salmeron and M. Mavrikakis, *Science*, 2023, **380**, 70–76.
40 R. Wang, H. Wang, X. Weng, J. Dai, Z. Gong, C. Zhao, J. Lu, Y. Cui and X. Bao, *J. Energy Chem.*, 2021, **60**, 150–155.
41 S. Jensen, M. H. R. Mammen, M. Hedevang, Z. Li, L. Lammich and J. V. Lauritsen, *Nat. Commun.*, 2024, **15**, 3865.
42 S. Kattel, P. Liu and J. G. Chen, *J. Am. Chem. Soc.*, 2017, **139**, 9739–9754.

43 J. A. Rodriguez, P. Liu, D. J. Stacchiola, S. D. Senanayake, M. G. White and J. G. Chen, *ACS Catal.*, 2015, **5**, 6696–6706.
44 J. Y. Han, J. Y. Yang, Z. X. Zhang, X. Z. Jiang, W. Liu, B. T. Qiao, J. J. Mu and F. Wang, *J. Am. Chem. Soc.*, 2023, **145**, 22671–22684.
45 C. R. A. Catlow, S. A. French, A. A. Sokol, M. Alfredsson and S. T. Bromley, *Faraday Discuss.*, 2003, **124**, 185–203.
46 C. Wu, L. Lin, J. Liu, J. Zhang, F. Zhang, T. Zhou, N. Rui, S. Yao, Y. Deng, F. Yang, W. Xu, J. Luo, Y. Zhao, B. Yan, X.-D. Wen, J. A. Rodriguez and D. Ma, *Nat. Commun.*, 2020, **11**, 5767.
47 F. Zhang, B. Li, X. Quan, K. Wang, J. Xu, T. Wu, Z. Li, M. Yan, S. Liu, Y. He, Y. Shi, Y. Su and P. Xie, *ACS Catal.*, 2024, **14**, 7136–7148.
48 X.-K. Wu, G.-J. Xia, Z. Huang, D. K. Rai, H. Zhao, J. Zhang, J. Yun and Y.-G. Wang, *Appl. Surf. Sci.*, 2020, **525**, 146481.
49 T. Reichenbach, K. Mondal, M. Jäger, T. Vent-Schmidt, D. Himmel, V. Dybbert, A. Bruix, I. Krossing, M. Walter and M. Moseler, *J. Catal.*, 2018, **360**, 168–174.
50 K. Mondal, Megha, A. Banerjee, A. Fortunelli, M. Walter and M. Moseler, *J. Phys. Chem. C*, 2021, **126**, 764–771.
51 W. Xiong, Z. F. Wu, X. Y. Chen, J. Q. Ding, A. A. I. Ye, W. H. Zhang and W. X. Huang, *Sci. China: Chem.*, 2023, **67**, 715–723.
52 X. Z. Wang, H. Zhang, H. Qin, K. M. Wu, K. Wang, J. F. Ma and W. D. Fan, *Fuel*, 2023, **346**, 128381.
53 Z.-J. Zuo, P.-D. Han, Z. Li, J.-S. Hu and W. Huang, *Appl. Surf. Sci.*, 2012, **261**, 640–646.
54 S. T. Bromley, S. A. French, A. A. Sokol, C. R. A. Catlow and P. Sherwood, *J. Phys. Chem. B*, 2003, **107**, 7045–7057.
55 K. Yao, S.-S. Wang, X.-K. Gu, H.-Y. Su and W.-X. Li, *Chin. J. Catal.*, 2013, **34**, 1705–1711.
56 J. Fu, S. Liu, W. Zheng, R. Huang, C. Wang, A. Lawal, K. Alexopoulos, S. Liu, Y. Wang, K. Yu, J. A. Boscoboinik, Y. Liu, X. Liu, A. I. Frenkel, O. A. Abdelrahman, R. J. Gorte, S. Caratzoulas and D. G. Vlachos, *Nat. Catal.*, 2022, **5**, 144–153.
57 G. Kresse and J. Furthmuller, *Phys. Rev. B: Condens. Matter Mater. Phys.*, 1996, **54**, 11169–11186.
58 G. Kresse and J. Furthmuller, *Comput. Mater. Sci.*, 1996, **6**, 15–50.
59 J. P. Perdew, K. Burke and M. Ernzerhof, *Phys. Rev. Lett.*, 1996, **77**, 3865–3868.
60 P. E. Blochl, *Phys. Rev. B: Condens. Matter Mater. Phys.*, 1994, **50**, 17953–17979.
61 G. Kresse and D. Joubert, *Phys. Rev. B: Condens. Matter Mater. Phys.*, 1999, **59**, 1758–1775.
62 T. Lunkenbein, J. Schumann, M. Behrens, R. Schlögl and M. G. Willinger, *Angew. Chem., Int. Ed.*, 2015, **54**, 4544–4548.
63 T. Song, R. Li, J. Wang, C. Dong, X. Feng, Y. Ning, R. Mu and Q. Fu, *Angew. Chem., Int. Ed.*, 2023, **63**, e202316888.
64 M. Mahapatra, J. Kang, P. J. Ramírez, R. Hamlyn, N. Rui, Z. Liu, I. Orozco, S. D. Senanayake and J. A. Rodriguez, *J. Phys. Chem. C*, 2018, **122**, 26554–26562.
65 V. Wang, N. Xu, J.-C. Liu, G. Tang and W.-T. Geng, *Comput. Phys. Commun.*, 2021, **267**, 108033.
66 G. Henkelman, B. P. Uberuaga and H. Jonsson, *J. Chem. Phys.*, 2000, **113**, 9901–9904.
67 G. Henkelman and H. Jonsson, *J. Chem. Phys.*, 2000, **113**, 9978–9985.
68 A. Heyden, A. T. Bell and F. J. Keil, *J. Chem. Phys.*, 2005, **123**, 224101.
69 *Materials Studio*, Biovia Software Inc., 5005 Wateridge Vista Drive, San Diego, CA 92121 USA, 2018.
70 Q.-L. Tang, W.-T. Zou, R.-K. Huang, Q. Wang and X.-X. Duan, *Phys. Chem. Chem. Phys.*, 2015, **17**, 7317–7333.
71 M. D. Higham, M. G. Quesne and C. R. A. Catlow, *Dalton Trans.*, 2020, **49**, 8478–8497.
72 Y.-F. Zhao, R. Rousseau, J. Li and D. Mei, *J. Phys. Chem. C*, 2012, **116**, 15952–15961.
73 V. Pallassana and M. Neurock, *J. Catal.*, 2000, **191**, 301–317.
74 T. Bligaard, J. K. Nørskov, S. Dahl, J. Matthiesen, C. H. Christensen and J. Sehested, *J. Catal.*, 2004, **224**, 206–217.
75 J. K. Nørskov, T. Bligaard, J. Rossmeisl and C. H. Christensen, *Nat. Chem.*, 2009, **1**, 37–46.
76 M. Heenemann, M.-M. Millet, F. Girgsdies, M. Eichelbaum, T. Risse, R. Schlögl, T. Jones and E. Frei, *ACS Catal.*, 2020, **10**, 5672–5680.
77 K. Larmier, W. C. Liao, S. Tada, E. Lam, R. Verel, A. Bansode, A. Urakawa, A. Comas-Vives and C. Coperet, *Angew. Chem., Int. Ed.*, 2017, **56**, 2318–2323.
78 Y. H. Wang, S. Kattel, W. G. Gao, K. Z. Li, P. Liu, J. G. G. Chen and H. Y. Wang, *Nat. Commun.*, 2019, **10**, 1166.
79 A. J. Medford, J. Sehested, J. Rossmeisl, I. Chorkendorff, F. Studt, J. K. Nørskov and P. G. Moses, *J. Catal.*, 2014, **309**, 397–407.
80 Y. Yang, J. Evans, J. A. Rodriguez, M. G. White and P. Liu, *Phys. Chem. Chem. Phys.*, 2010, **12**, 9909–9917.
81 L. C. Grabow and M. Mavrikakis, *ACS Catal.*, 2011, **1**, 365–384.
82 Y. Yang, C. A. Mims, D. H. Mei, C. H. F. Peden and C. T. Campbell, *J. Catal.*, 2013, **298**, 10–17.
83 S. Kattel, B. Yan, Y. Yang, J. G. Chen and P. Liu, *J. Am. Chem. Soc.*, 2016, **138**, 12440–12450.
84 L. Jiang, K. Liu, S.-F. Hung, L. Zhou, R. Qin, Q. Zhang, P. Liu, L. Gu, H. M. Chen, G. Fu and N. Zheng, *Nat. Nanotechnol.*, 2020, **15**, 848–853.
85 T. Yang, T. Gu, Y. Han, W. Wang, Y. Yu, Y. Zang, H. Zhang, B. Mao, Y. Li, B. Yang and Z. Liu, *J. Phys. Chem. C*, 2020, **124**, 27511–27518.
86 L. Song, X. Tian, Y. Yang, J. Qin, H. Li and X. Lin, *Front. Chem.*, 2020, **8**, 607.
87 K. C. Waugh, *Catal. Lett.*, 2012, **142**, 1153–1166.
88 G. C. Chinchen, P. J. Denny, D. G. Parkera, M. S. Spencer and D. A. Nhan, *Appl. Catal.*, 1987, **30**, 333–338.
89 G. C. Chinchen, P. J. Denny, J. R. Jennings, M. S. Spencer and K. C. Waugh, *Appl. Catal.*, 1988, **36**, 1–65.
90 Y.-F. Shi, P.-L. Kang, C. Shang and Z.-P. Liu, *J. Am. Chem. Soc.*, 2022, **144**, 13401–13414.
91 F. Studt, M. Behrens, E. L. Kunkes, N. Thomas, S. Zander, A. Tarasov, J. Schumann, E. Frei, J. B. Varley, F. Abild-Pedersen, J. K. Nørskov and R. Schlögl, *ChemCatChem*, 2015, **7**, 1105–1111.
92 Y.-F. Zhao, Y. Yang, C. Mims, C. H. F. Peden, J. Li and D. Mei, *J. Catal.*, 2011, **281**, 199–211.